A Six-Section Photonic Integrated Transmitter With Chirp Control for Extension of the Transmission Reach

Ankit Sharma, *Member, IEEE*, Aleksandra Maria Kaszubowska-Anandarajah, *Senior Member, IEEE*, Mohab Nabil Hammad, Michael Wallace, Jules Braddell, Frank Smyth, and Prince M. Anandarajah, *Senior Member, IEEE*

***Abstract*—We demonstrate a novel directly modulated transmitter, based on a six-section photonic integrated circuit. The device uses a unique master-slave configuration with a variable optical attenuator in between, allowing decoupling of cavities and independent control of the injection power. The VOA also provides the ability to find an optimum injection level that balances the trade-off between the extinction ratio and the chirp of the transmitted signal. Using the device, an error-free transmission of a 10 Gb/s non-return-to-zero signal over 25 km and 50 km standard single mode fibre is achieved.**

***Index Terms*—Photonic Integrated Circuits (PICs), Monolithic integrated circuits, Direct modulation, Chromatic dispersion.**

I. Introduction

THE epitaxial growth and integration of active and passive photonic components on a wafer delivers a suite of benefits such as dense packing of components, lower energy consumption, smaller footprint, improved performance and stability [1]. Photonic integrated circuits (PICs) have proven to be beneficial in a plethora of applications such as telecommunications, sensing, quantum computing and security [2]. All sectors of the telecommunications network benefit from the implementation of PICs, with the biggest benefit reaped in short reach networks, including access and datacenter networks. The use of PICs (transmitters and receivers) in these sectors can help meet the ever-growing capacity demand at a reduced cost and energy consumption, thus overcoming one of the biggest challenges in these segments.

In the access network, the ever-increasing bandwidth demand has led to the incorporation of wavelength division multiplexing (WDM) together with the traditional time division multiplexed approach, in a format known as time and wavelength division multiplexing (TWDM). The adopted standard, using the TWDM format, is realized by employing four distinct wavelengths, each operating at 10 Gb/s [3]. Such data rates can easily be achieved by using externally modulated lasers (EMLs), each operating at a different wavelength [4], [5]. However, one of the major drawbacks associated with the use of an EML transmitter is its high insertion loss and cost. A directly modulated laser (DML) transmitter is an attractive alternative, due to its simplicity and cost-effectiveness. However, one of the main challenges associated with DMLs stems from the modulation-induced frequency chirp, which severely limits the achievable transmission distances [6]. Optical injection locking (OIL) [7], a technique that is realized by arranging two lasers in master-slave configuration, can be used to reduce the chirp, while at the same time enhancing the modulation bandwidth (MBW) of the slave lasers [8]–[10]. By integrating both master and slave lasers in a single PIC, the advantages of the OIL can be exploited, while preserving the small footprint, energy saving, and cost effectiveness of the DML. The design of such structures becomes increasingly convenient due to the availability of multifunctional process design kits (PDKs).

Currently, there are two main integration platforms that are being used to develop PIC transceivers: III-V semiconductors and silicon photonics. Active PICs requiring gain and high-speed operation tend to use III-V (indium phosphide - InP) semiconductors [2], [11]. A major advantage with the use of InP is that it enables monolithic integration of the active (semiconductor optical amplifier, distributed feedback laser, distributed Bragg reflector) and passive (arrayed waveguide grating, splitter, waveguides) photonic building blocks [12]. The availability of the optimized PDKs allows for the realization of high-performance PICs. However, the complex PIC architectures increase the complexity of the fabrication process, requiring larger number manufacturing

Manuscript received 2 June 2022; accepted 23 June 2022. Date of publication 1 July 2022; date of current version 18 July 2022. This work was supported in part by research grants from the Irish Research Council EBPPG/2018/53, in part by the Science Foundation Ireland under Grants 15/CDA/3640, 12/RC/2077-P2, and 18/RI/5755, and in part by the DTIF under Grant DT20180268. *(Corresponding author: Ankit Sharma.)*

Ankit Sharma, Mohab Nabil Hammad, and Prince M. Anandarajah are with the Photonics Systems and Sensing Laboratory, School of Electronic Engineering, Dublin City University, D09 Dublin, Ireland (e-mail: ankit.sharma24@mail.dcu.ie; mohab.hammad2@mail.dcu.ie; prince.anandarajah@dcu.ie).

Aleksandra Maria Kaszubowska-Anandarajah is with the CONNECT Research Centre, Dunlop Oriel House, Trinity College Dublin, D02 Dublin, Ireland (e-mail: anandara@tcd.ie).

Michael Wallace is with the Pilot Photonics Ltd., D09 Dublin, Ireland, and also with Bright Photonics, 5612 AX Eindhoven, Netherlands (e-mail: wallacmj@tcd.ie).

Jules Braddell and Frank Smyth are with the Pilot Photonics Ltd., D09 Dublin, Ireland (e-mail: jules.braddell@pilotphotonics.com; frank.smyth@pilotphotonics.com).

Digital Object Identifier 10.1109/JPHOT.2022.3187073

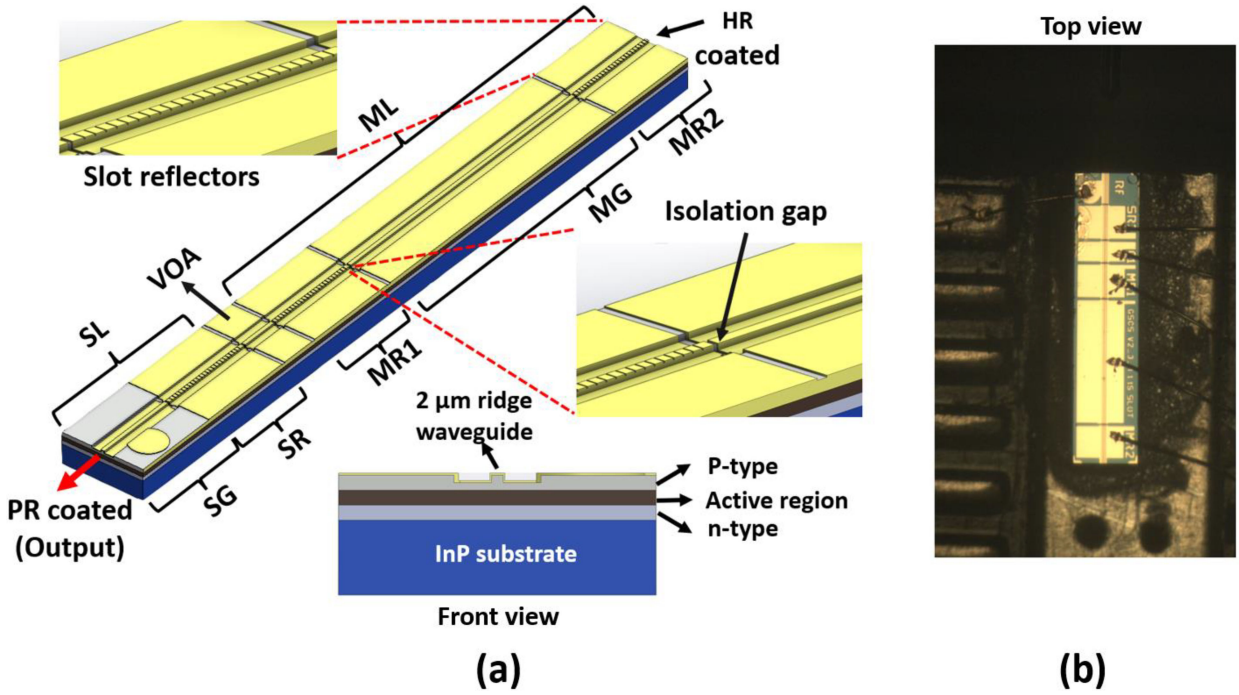

Fig. 1. (a) 3-D design of the 6-section PIC; inset: SL - slave laser, VOA - variable optical attenuator, ML - master laser, SG - slave gain, SR - slave reflector, MR - master reflector, MG - master gain, PR - partially reflective, and HR - highly reflective; and (b) is a photograph of the wire bonded PIC on a subcarrier.

runs (regrowth and etching process). This reduces the yield and results in an expensive and time-consuming fabrication process. Hence, the ability to use a simple regrowth-free fabrication procedure would go a long way towards improving the efficiency and reducing the cost of PIC manufacturing [13]–[15]. A monolithically integrated two section master-slave laser, fabricated using a regrowth free process, was used to demonstrate error free transmission of 10 Gb/s directly modulated data signals over 50 km of standard single mode fibre (SSMF) [16]. However, injection locking operation of this 2-section PIC transmitter proved to be very difficult due to coupled cavity effects. Another monolithically integrated mutually injection locked three-section DFB laser is demonstrated in [17]. The authors show a fourfold increase in the relaxation oscillation frequency. However, thermal crosstalk in the device led to challenges in achieving injection locking. More recently, a four-section master-slave PIC transmitter, also fabricated using a regrowth free process, was used to transmit a directly modulated 10 Gb/s data signal over 37 km of SSMF [18]. Here again, the 4-section PIC based transmitter suffered from multi-cavity coupling effects. In addition, due to the presence of a shared reflector, independent control of the various sections could not be achieved.

In this paper, we extend the work on a 6-section PIC device presented in [19], by carrying out a comprehensive characterisation of the device, improving the frequency response of the slave section, demonstrating independent control of the optical injection to mitigate the chirp when directly modulated, and extending the transmission distance. The device uses a high order surface grating etched into the ridge waveguide structure and thereby offers regrowth free manufacturing [18]. One section acts as a variable optical attenuator (VOA), which allows the optimization of the injection levels and thereby control of the chirp and the MBW. In addition, the VOA also enables independent control of the master and slave sections by reducing the coupled cavity effect. Finally, having an independent contact pad for each section helps to compensate thermal crosstalk with bias control. Experimental results achieved, reveal that under injection locking, such a device supports direct modulation at data rate of 10 Gb/s and the error free transmission of the modulated signal over 25 and 50 km spans of SSMF.

II. Device Design and Fabrication

The multi-section PIC transmitter (Fig. 1) was fabricated using a standard 1550 nm material, with 5 strained $Al_{(0.24)}Ga$-$In_{(0.71)}As$ quantum wells in the active region on an n-doped In-P substrate, as shown in the lower part of Fig. 1(a). A deeply etched 2 μm ridge waveguide confines the fundamental optical mode in the horizontal direction. The front facet of the PIC is partially reflective (PR) coated providing 33% reflectivity and the back facet has a highly reflective (HR) coating. The formation of multiple sections of the PIC, from a uniformly grown wafer, is achieved by etching the p-type material to a depth of 1.35 μm (as shown in the insets of Fig. 1(a)).

Fig. 1(b) shows a microscopic top view image of the PIC comprising six monolithically integrated sections i.e., the slave gain (SG), slave reflector (SR), VOA (G1), master reflector-1 (MR1), master gain (MG), and master reflector-2 (MR2) sections. The MR1, MG and MR2 sections constitute the master laser (ML). Similarly, the SG and SR section form the slave laser (SL). The length of ML and SL are 1263 μm and 430 μm. The SR, MR1, and MR2 reflectors are higher order slot gratings, as described

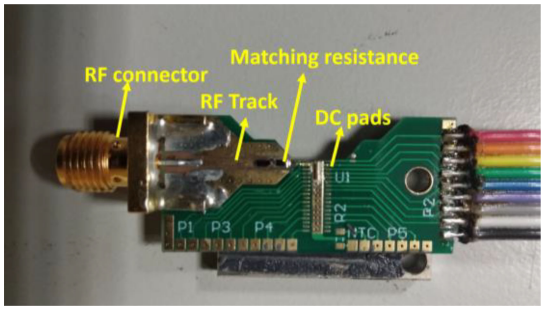

Fig. 2. Photograph of the PIC mounted on a PCB and wirebonded to electrical contacts.

in [20], with 1.15 μm wide etched slots in the ridge as shown in the inset of Fig. 1(a). It is important to note that the length of the G1 section is specifically optimised for its operation as a VOA. A $\sim$10 kΩ electrical isolation between the sections minimizes the current leakage and is achieved by designing slots between sections that are 1.35 μm deep and 10 μm wide.

A printed circuit board (PCB) with a radio frequency (RF) transmission line is designed and fabricated to characterize the PIC. First, a bare chip is placed and glued on to a PCB, after which the direct current (DC) and RF pads are wirebonded to the respective electrical contacts, as shown in Fig. 2. Thereafter, a matching resistance of 34 Ω is placed in series with the SG section and 50 Ω RF track. In order to maintain the PIC at a fixed temperature of 18 °C throughout the entire characterisation and system experiment, a thermoelectric cooler (TEC) is placed under the PCB together with a temperature sensor (thermistor). The TEC is driven with a proportional-integral-derivative (PID) temperature controller. The DC pads of the PCB are connected to low noise DC current sources, while the SG section is connected to a wideband bias tee (BT) with a bandwidth spanning from DC to 10 GHz. The light from the PIC based transmitter is coupled with the aid of a conical lensed fibre, mounted on an auto-aligner. The output of the lensed fibre is split using a 90:10 coupler, with 10% used as feedback to the auto-aligner controller and 90% used for the static and dynamic characterization, and for the transmission experiment.

III. Static Characterization of the PIC

To carry out the static characterization of the device, the SL sections were first biased individually, while keeping the remaining sections unbiased. Initially, the total output power of the SL is measured while sweeping the currents of the SG from 0 to 80 mA and the SR sections from 4 mA to 60 mA in 4 mA steps.

The results are plotted in Fig. 3. From the plots, it can be seen that the SL emits 0.5 mW of power and shows a linear region suitable for direct modulation when the SR section is biased at 56 mA and the SG section at 40 mA. The maximum power is achieved when the SR is biased at 56 mA and the SG at 42 mA. Beyond the SG bias of 42 mA, the output power drops, due to the longitudinal mode of the SL not lying within the reflectance band of the SR grating.

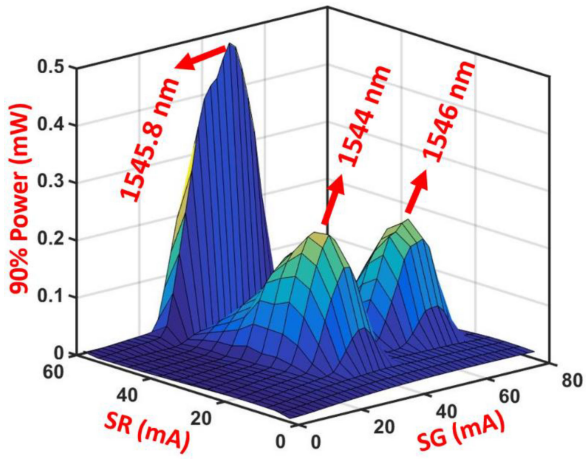

Fig. 3. L-I plot of the SL at various SG and SR currents.

The next characterisation step entailed obtaining heat maps of the wavelength and the side mode suppression ratio (SMSR) of the SL as a function of the SR and SG currents. This was achieved by sweeping the SG current between 0 and 80 mA and the SR current between 10 and 80 mA in steps of 2 mA whilst measuring the SMSR and peak wavelength at resolution of 20 pm with the aid of an optical spectrum analyser (OSA).

Fig. 4(a) indicates that the wavelength of the SL can be tuned from 1543 nm to 1548 nm. In addition, the wavelength map confirms a mode hop (switching between longitudinal modes indicated by an abrupt change in colour in the wavelength map) as the main reason for the drop in power (shown in Fig. 3), when the SR is biased between 45 and 70 mA. It is important to note that the few dots seen in the lower left hand side of Fig. 4(a) are a measurement artefact. Fig. 4(b) clearly shows that the wavelength range between 1545 nm and 1547 nm achieves an SMSR of more than 45 dB. In addition, Fig. 4(c) shows the SMSR as a function of the slave laser emission wavelength (from 1544 to 1546 nm), achieved by extracting all wavelengths that exhibit an SMSR of 35 dB and above. An optical spectrum of the SL, captured at bias currents of SG $=$ 38 mA and SR $=$ 40 mA, is shown in Fig. 5(a) (spectral resolution of 0.16 pm).

Next, we verify the independent lasing of the ML by biasing the SL and VOA at transparency (SR, SG and VOA biased at 14 mA, 14 mA, and 10 mA respectively), while the ML sections (MR1, MG, MR2) are biased at 52 mA, 100 mA, and 60.33 mA, respectively. At this operating point, the ML is seen to be lasing at $\sim$ 1547 nm (Fig. 5(b)). As expected and based on the lengths of the respective sections, the spectra in Fig. 5 clearly show that the ML (Fig. 5(b)) exhibits much better spectral purity in comparison to the SL (Fig. 5(a)).

IV. Optical Injection Locking

Having characterised the individual SL and ML lasers, the next step is to verify the ability to achieve optical injection locking (OIL) of the SL by the ML. This process is started by turning-on the SL sections and VOA (the SG, SR, and VOA are biased at 50 mA, 60 mA, and 10 mA, respectively), while the

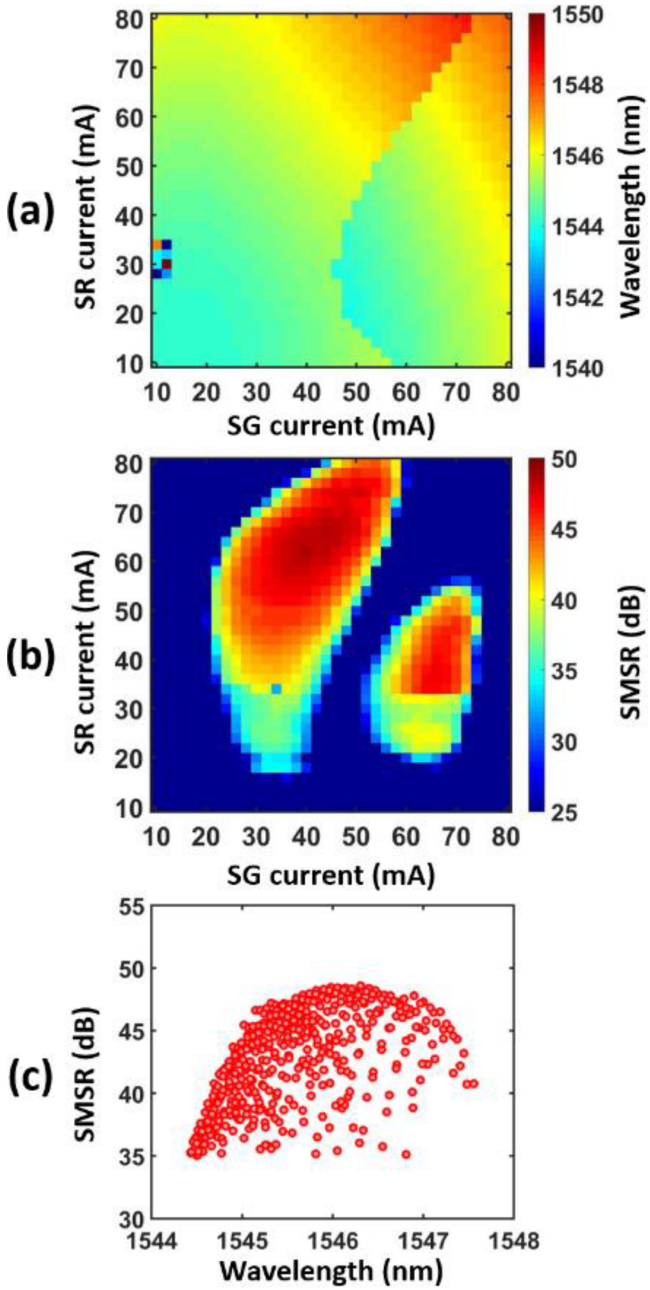

Fig. 4. Heat maps of the (a) wavelength of the SL as a function of the SR and SG currents, (b) Side mode suppression ratio (SMSR) and (c) plot of wavelengths at SMSR greater than or equal to 35 dB.

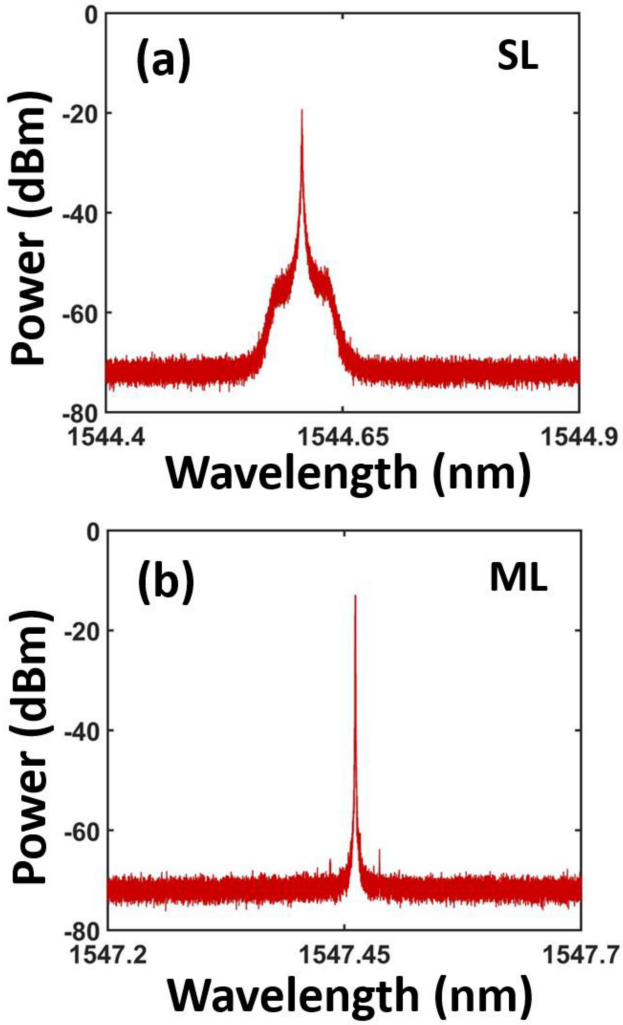

Fig. 5. Optical spectrum (a) of the SL when the VOA and ML are off, and (b) of the ML when the SL and VOA are biased at transparency.

ML emission is tuned from 1545.48 nm to 1547.56 nm. The latter is achieved by varying the bias currents of both gratings (tied together) and the MG sections between 0 mA to 68 mA (in 2 mA steps) and measuring the output SMSR on an OSA. The results achieved are plotted, as a heat map of the SMSR as a function of the MR current (MR1 and 2 are tied together) and the MG current, in Fig. 6(a). The high SMSR regions (red areas in Fig. 6(a)) indicate a high probability of achieving optical injection locking. Based on these results, an MG bias of 35 mA is selected.

Having chosen an optimum bias point for MG, the next step entailed finding similar optimum bias currents for MR1 and MR2 sections. Hence, with the MG section biased at 35 mA, the biases supplied to MR1 and MR2 are varied individually from 0 to 68 mA in steps of 2 mA. The results achieved are then plotted as a heat map of the SMSR as a function of the two MR currents with a fixed MG current and shown in Fig. 6(b). The regions with an SMSR $>$ 55 dB (dark red region in Fig. 6(b)) clearly indicate that OIL is achieved. Hence, a set of bias currents, which lead to OIL, can be deduced from Fig. 6(b). An example of a spectrum of the injection locked SL for bias currents given in Table I (gleaned from Fig. 6(b)), is shown in Fig. 7.

The stability of the injection-locked wavelength is determined by measuring peak wavelength using a high-resolution (0.16 pm) OSA. A python script is written to extract the peak wavelength from the OSA at one-minute intervals. A maximum deviation of $\sim$282 MHz is observed over 60 minutes of observation. The injection-locked wavelength can be tuned by ~ 4.6 pm (tuning resolution). In addition, the injection-locked

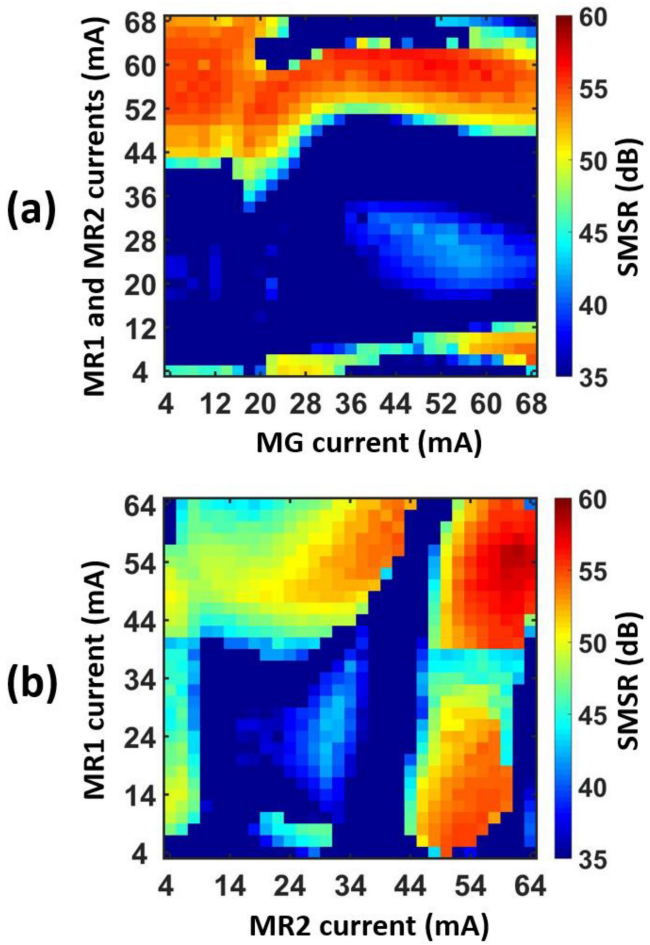

Fig. 6. Heat maps of (a) SMSR data versus MG current at different MR1 and MR2 currents, and (b) SMSR data at versus a fixed MG current and 2-dimensional independent sweeping of MR1 and MR2 currents.

TABLE I
OPERATING CONDITION OF PIC IN OIL MODE

Section	Current (mA)
SR	50.72
SG	57.54
VOA	10
MR1	54.12
MG	35
MR1	56.17
Temperature	18°C

Table I Section currents for injection locked SL shown in Fig. 7.

wavelength can be tuned by a maximum of 75 GHz by changing the SR, MR1, and MR2 currents while keeping SG, VOA, and MG currents unchanged.

V. DYNAMIC CHARACTERIZATION

In this section, the modulation response of the optically injection locked SL is investigated. It is well known that the resonance frequency of the SL under optical injection is directly proportional to the ratio of injected optical power to power of the free running SL [21]. Hence, the measurements are carried out

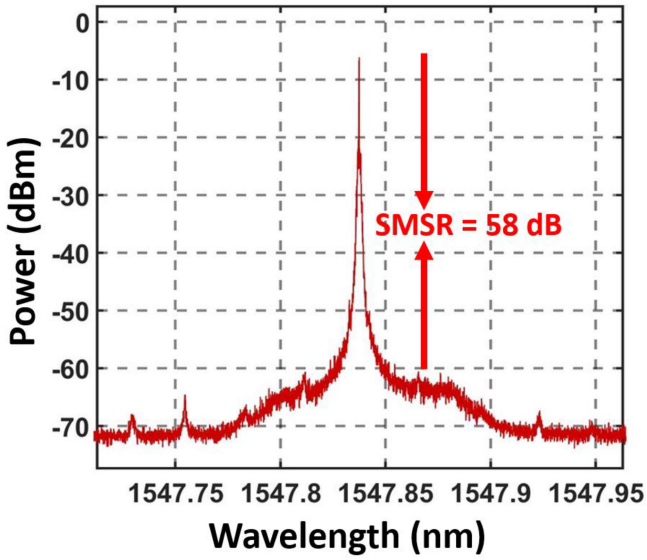

Fig. 7. Optical spectrum of the injection locked SL (OSA resolution of 0.16 pm).

for different levels of injected power. It is important to note that the optical injection in this device can be varied in two ways: by changing the MG current, which results in a change of the ML output power or by changing the attenuation level of the VOA. However, changing of the MG bias current results in a change of its wavelength. Hence, the second option is chosen.

The bias current applied to the VOA is tuned to change its state from opaque to transparent. As the VOA section is made of an active material, transparency is achieved by supplying sufficient current to compensate for the waveguide loss. Thus, by changing the bias to the VOA section, the level of the optical injection from the ML to SL can be varied. The next step involves measuring the frequency response of the slave laser at different biases applied to the VOA section. The operating condition for the PIC are chosen from Table I except for the VOA section current, which is tuned between 1 and 12 mA.

The frequency response (S_{21}) of the SL section is plotted and shown in Fig. 8. The blue line depicts the case where there is little or no injection from the ML (VOA section bias is set to 0 mA (turned-off)). The 3-dB MBW in this operating condition is measured to $\sim$ 3.6 GHz. When the current to the VOA section (thus the optical injection) is increased, the 3-dB MBW improves, reaching $\sim$ 4.6 GHz at 1 mA (orange line) and finally $\sim$7.8 GHz, when the VOA section current is set at 12 mA (cyan line).

VI. DIRECT DATA MODULATION AND TRANSMISSION

Finally, we carried out direct modulation of the multi-section PIC, using the experimental setup shown in Fig. 9. Once again, the bias currents shown in Table I are used. A $2V_{pp}$, non-return-to-zero, pseudo random bit sequence $(2^{15}-1)$ at 10 Gb/s from a pulse pattern generator (PPG) is applied to the SG section of the laser, in conjunction with a DC current. The output signal of the PIC is split using 90:10 coupler, with the 10% tap connected

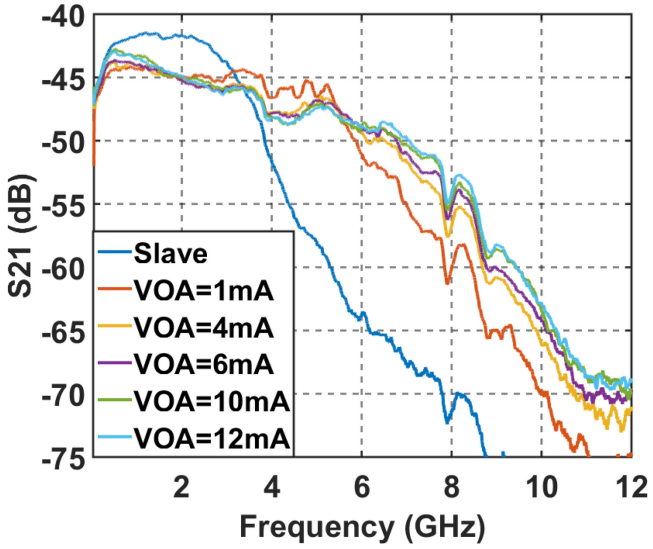

Fig. 8. Frequency response of optically injected SL at different VOA currents.

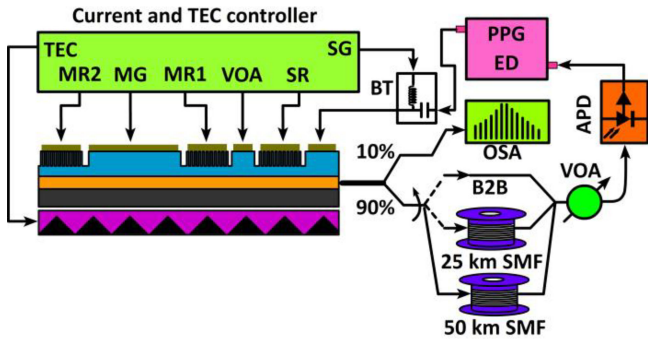

Fig. 9. Experimental setup used for the direct modulation of the PIC.

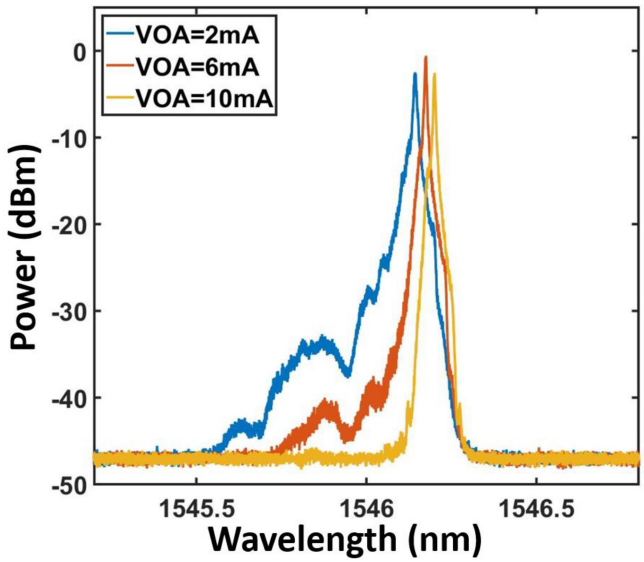

Fig. 10. Optical spectra of the directly modulated slave section with VOA section bias set to 2 mA (blue), 6 mA (orange), and 10 mA (yellow).

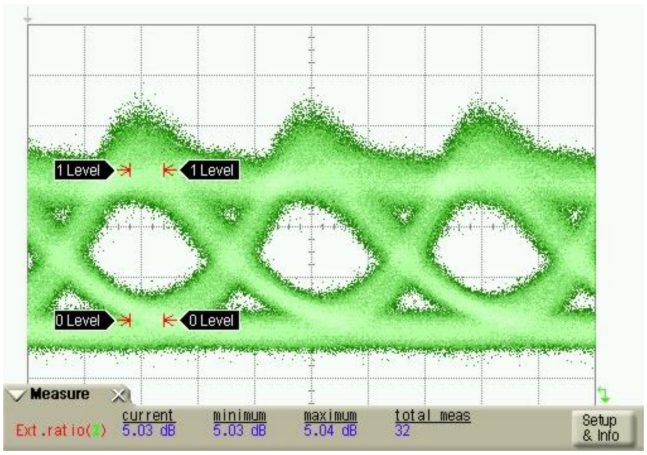

Fig. 11. Eye diagram of the received signal in a B2B case and the measurement of its ER.

to the OSA and the 90% tap launched into a patch cord (back-to-back), 25 km or a 50 km reel of SSMF. The received signal is passed through an external VOA, to change the received optical power (ROP), prior to being fed to an avalanche photodiode (APD). The output of the APD is connected to the error detector (ED) for bit error rate (BER) analysis.

The narrowing of the optical spectrum of the modulated signal, shown in Fig. 10, shows that the in-chip optical injection can significantly reduce the frequency chirp induced by the direct modulation. Furthermore, the amount of chirp can be controlled by adjusting the bias of the VOA section. It is important to note that the optical injection also results in a reduction of the extinction ratio (ER) of the modulated signal. Hence, there is a trade-off between the level of chirp compensation and the degradation of the ER. In other words, a shorter transmission distance (less dispersion) could benefit from a reduced level of optical injection (better ER).

The eye diagram of the received optical signal in a back-to-back scenario is shown in Fig. 11. From the plot we measure the extinction ration (ER) of the signal to be ~ 5 dB.

Next, we measure the BER, as a function of the ROP, of the received signal for the back-to-back case and after transmission over 25 km and 50 km of SSMF. The BER plots are shown in Fig. 12. An error free transmission ($1e^{-9}$) is achieved for all three scenarios. The receiver sensitivity ($1e^{-9}$) is measured to be -22 dBm for the 25 km and -15 dBm for the 50 km fibre transmission . This corresponds to a power penalty, with respect to the back-to-back case, of ~ 2 dB (25 km) and ~ 5 dB(50 km), which can be attributed to the chromatic dispersion incurred in the fibre.

Finally, to demonstrate the effectiveness of the VOA and the advantage of optical injection, we measure the effect of varying the VOA current on the BER performance for the two transmission distances of 25 and 50 km. From the results, plotted in Fig. 13, it can be seen that by increasing the VOA bias, thus the injection level, a significant improvement in the performance of the system can be achieved. In the case of the 25 km transmission, changing the VOA section current from 4.5 mA to 10 mA reduces the BER from $1e^{-3}$ to $1e^{-9}$.

Similarly, in the case of the 50 km transmission, changing the VOA section current from 4.5 mA to 12 mA also reduces the

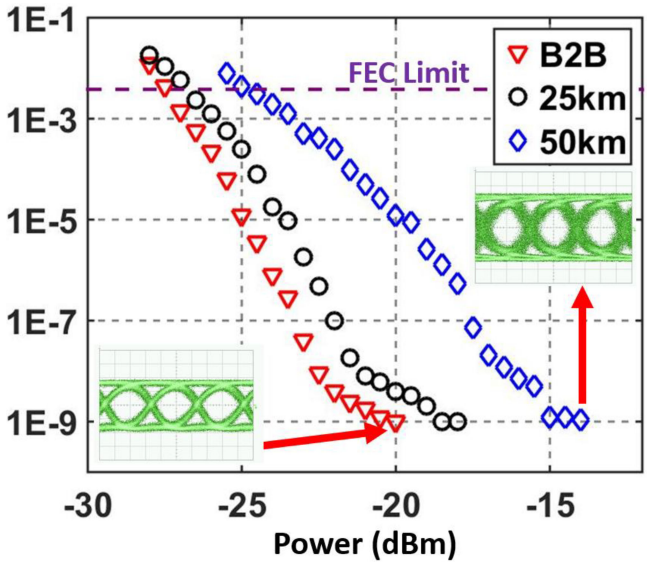

Fig. 12. BER vs. ROP for back-to-back and after transmission over 25 and 50 km of SSMF, inset: eye diagrams at the indicated BER.

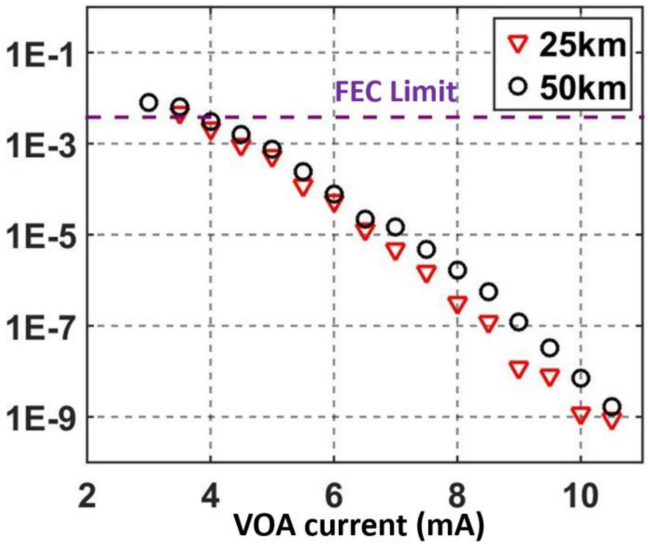

Fig. 13. BER vs. VOA current after transmission over 25 km and 50 km.

BER from $1e^{-3}$ to $1e^{-9}$. This BER improvement stems from the reduction of the chirp induced by the optical injection. It also shows that for the longer fibre length, optimising the system performance requires a higher level of injection (higher VOA current).

VII. Conclusion

A 6-section PIC with a novel design is demonstrated as a 10 Gb/s directly modulated transmitter. The unique architecture of the device is based on the introduction of an integrated VOA between the master and slave laser sections. The VOA simplifies the control of the injection levels by mitigating the coupled cavity effects, avoiding changes in the wavelength and enabling a trade-off between the ER degradation, MBW enhancement and chirp reduction introduced by optical injection. The VOA managed optimization of injection enables error free transmission of a directly modulated 10 Gb/s signal over 25 km and 50 km of SSMF. This re-growth free multi-section device can prove to be a cost-effective transmitter for employment in next generation access networks.

References

[1] M. Smit *et al.*, "An introduction to InP-based generic integration technology," *Semicond. Sci. Technol.*, vol. 29, no. 8, 2014, Art. no. 083001.
[2] S. Arafin and L. A. Coldren, "Advanced InP photonic integrated circuits for communication and sensing," *IEEE J. Sel. Topics Quantum Electron.*, vol. 24, no. 1, Jan./Feb. 2018, Art. no. 6100612.
[3] ITU.int.G.989.2, "40-Gigabit-capable passive optical networks 2 (NG-PON2): Physical media dependent (PMD) layer specification," 2022. Accessed: Jul. 6, 2022. [Online]. Available: https://www.itu.int/rec/T-REC-G.989.2-201902-I
[4] W. Yao, M. K. Smit, and M. J. Wale, "High-density monolithic 6×30 Gb/s tunable WDM transmitter in generic III-V platform," in *Proc. Conf. Lasers Electro-Opt. Pacific Rim*, Jul. 2017, pp. 1–2. doi: 10.1109/CLEOPR.2017.8118940.
[5] B. Huang, Z. Zhang, Z. Zhang, C. Cheng, and H. Chen, "100Gb/s ultra wide misalignment tolerance WDM transmitter with novel vertical grating coupler," in *Proc. IEEE Photon. Soc. Summer Topical Meeting Ser.*, Jul. 2017, pp. 75–76, doi: 10.1109/PHOSST.2017.8012657.
[6] K. Sato, S. Kuwahara, and Y. Miyamoto, "Chirp characteristics of 40-Gb/s directly modulated distributed-feedback laser diodes," *J. Lightw. Technol.*, vol. 23, no. 11, pp. 3790–3797, Nov. 2005, doi: 10.1109/JLT.2005.857753.
[7] Z. Liu and R. Slavík, "Optical injection locking: From principle to applications," *J. Lightw. Technol.*, vol. 38, no. 1, pp. 43–59, Jan. 2020.
[8] S. Mohrdiek, H. Burkhard, and H. Walter, "Chirp reduction of directly modulated semiconductor lasers at 10 Gb/s by strong CW light injection," *J. Lightw. Technol.*, vol. 12, no. 3, pp. 418–424, Mar. 1994.
[9] G. Yabre, "Effect of relatively strong light injection on the chirp-to-power ratio and the 3 dB bandwidth of directly modulated semiconductor lasers," *J. Lightw. Technol.*, vol. 14, no. 10, pp. 2367–2373, Oct. 1996.
[10] Y. Mao *et al.*, "Modulation bandwidth enhancement and chirp reduction in DFB lasers with active optical feedback," in *Proc. Conf. Lasers Electro-Opt.*, 2019, Paper JTu2A.70.
[11] G. Raghavan, M. Sokolich, and W. E. Stanchina, "Indium phosphide ICs unleash the high-frequency spectrum," *IEEE Spectr.*, vol. 37, no. 10, pp. 47–52, Oct. 2000.
[12] L. M. Augustin *et al.*, "InP-based generic foundry platform for photonic integrated circuits," *IEEE J. Sel. Topics Quantum Electron.*, vol. 24, no. 1, Jan./Feb. 2018, Art. no. 6100210.
[13] V. Tolstikhin, "Multi-guide vertical integration in InP: PIC technology for cost-sensitive applications," in *Proc. Conf. Lasers Electro-Opt./Pacific Rim*, 2013, Paper TuN1_3.
[14] S. P. Duggan, "Regrowth-free monolithic vertical integration of passive and active waveguides," Ph.D. dissertation, Univ. College Cork, Cork, Ireland, 2019.
[15] N. P. Kelly, "Monolithic integration of photonic devices for use in a regrowth-free coherent WDM transmitter," Ph.D. dissertation, Univ. College Cork, Cork, Ireland, 2017.
[16] J. O'Carroll *et al.*, "Transmission over 50 km using a directly modulated integrated two-section discrete mode laser at 1550 nm," in *Proc. Conf. Lasers Electro-Opt. Europe Int. Quantum Electron. Conf.*, May 2013, pp. 1–1. doi: 10.1109/CLEOE-IQEC.2013.6800721.
[17] C. Sun *et al.*, "Modulation characteristics enhancement of monolithically integrated laser diodes under mutual injection locking," *IEEE J. Sel. Topics Quantum Electron.*, vol. 21, no. 6, Nov./Dec. 2015, Art. no. 1802008, doi: 10.1109/JSTQE.2015.2478817.
[18] G. Jain *et al.*, "Directly modulated photonic integrated multi-section laser for next generation TWDM access networks," in *Proc. 45th Eur. Conf. Opt. Commun.*, 2019, pp. 1–4.
[19] A. Sharma *et al.*, "A six-section photonic integrated transmitter with chirp control for transmission reach extension," in *Proc. 27th Int. Semicond. Laser Conf.*, 2021, pp. 1–2.
[20] Q. Lu, W.-H. Guo, D. Byrne, and J. F. Donegan, "Design of slotted single-mode lasers suitable for photonic integration," *IEEE Photon. Technol. Lett.*, vol. 22, no. 11, pp. 787–789, Jun. 2010, doi: 10.1109/LPT.2010.2045888.
[21] H.-K. Sung, E. K. Lau, and M. C. Wu, "Optical properties and modulation characteristics of ultra-strong injection-locked distributed feedback lasers," *IEEE J. Sel. Topics Quantum Electron.*, vol. 13, no. 5, pp. 1215–1221, Sep./Oct. 2007.